

# CFD Research Corporation

215 Wynn Dr. • Huntsville, Alabama 35805 • Tel.: (256) 726-4800 • FAX: (256) 726-4806 • info@cfdrcc.com



## AN ADVANCED CAD TOOL FOR QUANTUM DEVICE SIMULATION

### Progress Report

(June 1, 1999 - July 31, 1999)

by

**P. Stout and A. J. Przekwas**  
CFD Research Corporation

**G. Klimeck and R. C. Bowen**  
Jet Propulsion Laboratory

**DISTRIBUTION STATEMENT A**  
Approved for Public Release  
Distribution Unlimited

August 1999

CFDRC Report: 8204-99/2

19990813 047

**Office of Naval Research**  
**ONR25, Code251**  
**Ballston Tower One**  
**800 North Quincy Street**  
**Arlington, VA 22217-5660**  
**Contract Number: N00014-99-M-0181**

R&D Services and Software for Computational Fluid Dynamics (CFD)

Branch Office: 2 Lakeview Ave., Suite 200 • Piscataway, New Jersey 08854 • Tel.: (732) 424-9393 FAX: (732) 424-9399

**DTIC QUALITY INSPECTED 4**

## 1. INTRODUCTION

This report describes the technical progress on the Office of Naval Research Project (Contract # N00014-99-M-0181) entitled "An advanced CAD tool for quantum device simulation". The current reporting period is June 1, 1999 through July 31, 1999.

## 2. TECHNICAL PROGRESS

The significant achievements during the second and third month of the project include: a CFDRC employee receiving three weeks of training on the NEMO theory and software at JPL, implementing a single band model that sits on identical footing to all NEMO multiband models, an initial implementation of small signal AC analysis for 1, 2, and 10 band tight binding models, grouping the 960+ source files into a library oriented directory tree, establishing a CVS repository of the NEMO source code to facilitate co-development, implementing a new build system to compile and link the NEMO source, porting NEMO to the DEC platform, and writing a "moving average" routine which averages quantities on disparate x,y plots onto a common incremented axis. The accomplishments under the appropriate task are described below.

### **Task 1. Implement AC small signal analysis in an existing quantum simulator (NEMO) through S-parameter extraction**

#### **Single Band Model**

A single band model was implemented which sits on identical footing to all of the NEMO multiband models. The implementation of the new AC model is basically an expansion of the orbital bases such as  $sp^3s^*$  by a factor of three to include the center energy and one absorption and one emission sideband. So all the multiband matrix sizes (e.g.  $sp^3s^*$  is of size  $10 \times 10$ , consisting of 5 orbitals and 2 spins) will triple. For debugging purposes one wants to keep the matrix sizes as small as possible to achieve fast turn-around within the framework of simplified physics. Dealing with a single-band model within the multiband framework would mean operating on  $1 \times 1$  matrices, which is rather inefficient. That is why the no-scattering single-band models were historically de-coupled from the multiband models. Within a single band AC simulation the matrix sizes are  $3 \times 3$  which would fit well into the multiband framework. To enable fast debugging we implemented a single band model fully into the NEMO multiband framework. This single band model is subject to modification by the AC radiation in the same way as all other bandstructure models.

#### **Small Signal AC Analysis for 1, 2, and 10 Band Tight Binding Models**

The largest theory and software development task this reporting period was the extension of the existing NEMO code to small signal AC analysis. NEMO was developed under government funding by Raytheon / TI for the *quantitative* analysis of resonant tunneling diodes. NEMO is presently the only quantum device design and analysis code that can predict and analyze the performance of *realistically extended* tunneling structures including the effects of contacts, scattering and bandstructure. The generality and comprehensiveness of NEMO stem from the non-equilibrium Green function theoretical approach. This approach allows for a general treatment of injection from accumulated emitters, inelastic scattering and realistic bandstructure models. No other approach, e.g. Density matrix, Wigner function or Schrödinger equation, has

equaled the success of NEMO for the simulation of DC current through realistically extended resonant tunneling diodes. For reference we have included several simulation examples that were generated previously.

The original NEMO theory and software had been limited to the time independent, steady state, DC analysis. The argument for this limitation was: "Let's get the DC part right first!" While other approaches have been implemented for true time dependent simulation or small signal AC analysis, none could really predict the DC characteristics of industry relevant resonant tunneling diodes. During this reporting period the implementation of small signal AC signal analysis into the NEMO theory and software framework has started.

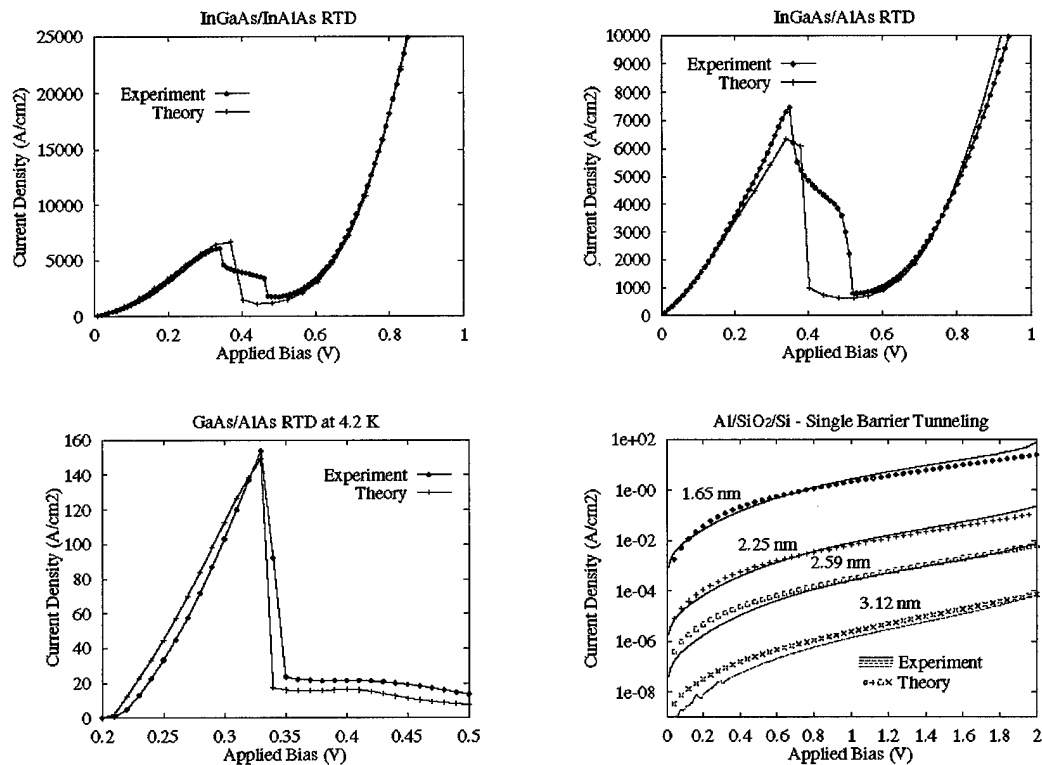


Figure 1. I-V simulations for four different classes of tunneling devices obtained using NEMO in previous work. The simulations are compared to experimental data. (a) InGaAs/InAlAs lattice-matched RTD at room temperature. Simulation is based on a full-band, quantum-charge self-consistent  $sp^3s^*$  model without scattering. (b) High performance InGaAs/AlAs pseudomorphic strained RTD at room temperature. Simulation model is the same as in (a). (c) GaAs/AlAs RTD at 4.2 K showing a scattering-assisted valley current (phonon peak). The single-band simulation includes scattering caused by polar optical phonons, interface roughness, and acoustic phonons. Band structure effects can be ignored in this device at low temperature. (d) Si/SiO<sub>2</sub>/Al single-barrier structure. Simulation is based on a single-band model.

An AC potential is included in the Hamiltonian by adding the matrix elements of a sinusoidal perturbation. These matrix elements result in the generation of harmonics whose first order coefficients provide AC conductance and susceptance. The matrix elements of the DC Hamiltonian in NEMO is represented as follows,

$$\langle \alpha, L, k | H^{DC} | \alpha', L', k \rangle = D_{\alpha, \alpha'}^{DC}(k) \delta_{L, L'} - t_{\alpha, L; \alpha', L'}^{DC}(k) \delta_{L, L' \pm 1}$$

The submatrices  $D^{DC}$  and  $t^{DC}$  are of the order of the basis of the bandstructure model. The diagonal block contains the on-site orbital energies and the electrostatic potential while the off diagonal block contains site to site interaction energies. The addition of an AC perturbation results in coupled harmonic sidebands. The AC Hamiltonian including only the first order harmonics may be expressed as follows:

$$D^{AC} = \begin{bmatrix} D^{DC} - \hbar\omega & \frac{v^{AC}}{2} I \\ & D^{DC} \\ \frac{v^{AC}}{2} I & D^{DC} + \hbar\omega \end{bmatrix}$$

$$t^{AC} = \begin{bmatrix} t^{DC} & & \\ & t^{DC} & \\ & & t^{DC} \end{bmatrix}$$

where  $\omega$  is the frequency and  $v^{AC}$  is the magnitude of the perturbation. In NEMO all physical observables are calculated using the retarded Green's function. The retarded Green's function for a three monolayer device takes the following mathematical form.

$$G^R = \begin{bmatrix} E - D_1^{AC} - \Sigma_{1,1}^{RB} & t_{1,2}^{AC} & \\ t_{2,1}^{AC} & E - D_2^{AC} & t_{2,3}^{AC} \\ & t_{3,2}^{AC} & E - D_3^{AC} - \Sigma_{3,3}^{RB} \end{bmatrix}^{-1}$$

The boundary self-energies,  $\Sigma^{RB}$ , couple electrons within the device to contact reservoirs assumed to be in thermal equilibrium. For the AC case the boundary self-energies take the form,

$$\Sigma_{1,1}^{RB} = - \begin{bmatrix} t_{0,1}^{DC} & & \\ & t_{0,1}^{DC} & \\ & & t_{0,1}^{DC} \end{bmatrix} \begin{bmatrix} J'_0 \chi_{-\hbar\omega} Z_{-\hbar\omega} \chi_{-\hbar\omega}^{-1} & J'_{-1} \chi_{-\hbar\omega} Z_{-\hbar\omega} \chi_{-\hbar\omega}^{-1} & J'_{-2} \chi_{-\hbar\omega} Z_{-\hbar\omega} \chi_{-\hbar\omega}^{-1} \\ J'_1 \chi_0 Z_0 \chi_0^{-1} & J'_0 \chi_0 Z_0 \chi_0^{-1} & J'_{-1} \chi_0 Z_0 \chi_0^{-1} \\ J'_2 \chi_{+\hbar\omega} Z_{+\hbar\omega} \chi_{+\hbar\omega}^{-1} & J'_1 \chi_{+\hbar\omega} Z_{+\hbar\omega} \chi_{+\hbar\omega}^{-1} & J'_0 \chi_{+\hbar\omega} Z_{+\hbar\omega} \chi_{+\hbar\omega}^{-1} \end{bmatrix}$$

$$J'_m = J_m(v^{AC} / \hbar\omega)$$

where  $J_m$  is the Bessel function of the first kind. The matrix  $Z_{AE}$  is a diagonal matrix of Bloch propagation factors for the bulk DC Hamiltonian shifted by energy  $\Delta E$ . The columns of the matrix  $\chi_{AE}$  contain the corresponding Bloch eigenvectors. The data structures in NEMO have been designed to implement the mathematics required for AC calculations in a general object-oriented manner. This allows one to perform AC simulations using NEMO's entire suite of sophisticated models.

The numerical AC simulation capability has been prototyped with three different bandstructure models: the single band model, the 2 band  $k \cdot p$  model, and the 10 band  $sp^3s^*$  tight binding model. These three bandstructure models augmented by a photon/radiation emission and absorption sideband now show up as additional bandstructure choices throughout the NEMO code. All the previously developed numerical tools such as resonance finding, grid generation, bandstructure computation and data visualization are now also available to the use in the AC simulation.

## **Task 2. Demonstration/Validation Studies of Resonant Tunneling Diodes (RTDs)**

The initial testing of the small signal AC implementation for a single band model consisted of checking for 1) proper transmission through a bulk semiconductor, 2) current conservation throughout the structure, and 3) proper transmission through a simple RTD. Tests 1 and 2 resulted in the expected flat lines of transmission coefficient versus energy or current density versus space, respectively.

Figures 2 - 5 show the first small signal AC results for a RTD obtained with a single band model using one photon emission and one photon absorption sideband. Figure 2a shows the conduction band edge of a simple InGaAs/InAlAs RTD and the three computed resonances in the center of the device. The three resonances are the RTD ground state surrounded by one sideband above and below separated by a photon energy of 10meV. Figure 2b shows two corresponding transmission coefficients traces as a function of energy. One transmission coefficient results from the tracing of the whole basis set, which implies equal electron injection into all three channels from the leads. The transmission peaks are in alignment with the resonances of Figure 2a. Since the tails of these three independent bands overlap, a transmission coefficient of greater than one can be achieved. However, electrons are only injected into the center band from the contact and may be transferred to the sidebands by the AC radiation / photons. Given a weak field the transmission coefficient will only show a single peak of maximum amplitude one.

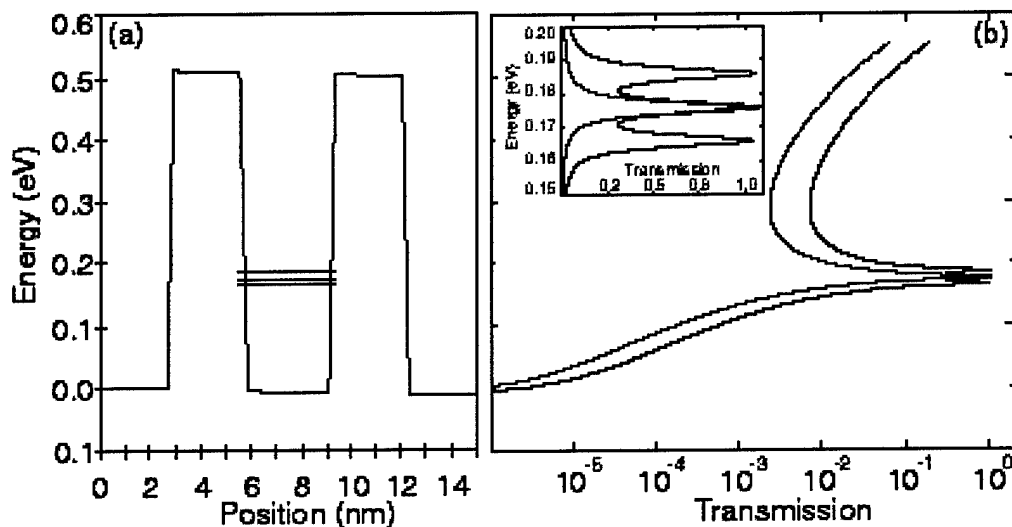


Figure 2. (a) Conduction band edge of a InGaAs/InAlAs RTD showing the center resonance in red and two sidebands in separated by 10meV in blue. (b) Transmission coefficients as a function of energy. Black line: equal electron injection from the contacts into three bands. Overlap of the bands can result in transmission coefficients greater than one. Red line: Electron injection from the contacts only into the center band. Transmission is again normalized to one. Insert: zoom around the resonance energy on a linear scale.

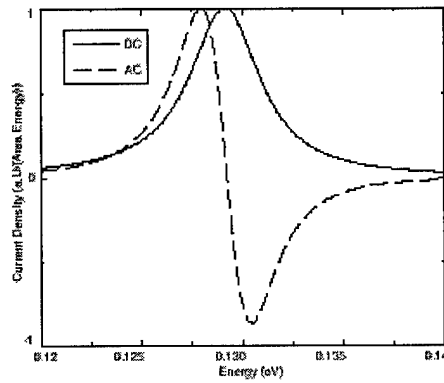


Figure 3. First order harmonics due to an AC perturbation on an RTD. DC component shows Lorentz lineshape as transmission of Figure 2b. AC component shows the principal value-type behavior to DC component.

Following the current conservation and transmission coefficient test the spectral behavior of the AC harmonics need to be verified. Figure 3 shows the real parts of the current density for the DC and the AC component as a function of energy. The DC current density shows the Lorentzian lineshape already shown in Figure 2. The corresponding AC component shows a principal value type lineshape to the original DC excitation.

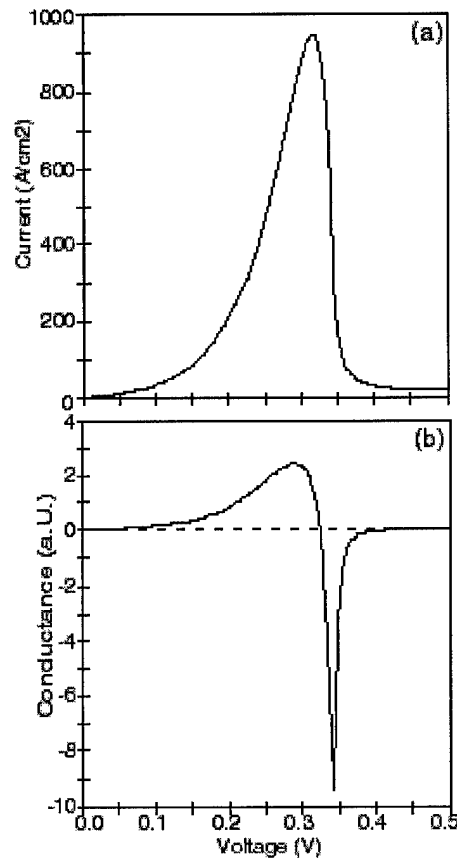


Figure 4. (a) DC Current-voltage characteristic for the RTD structure of Figure 2. (b) AC small signal conductance for small excitation frequencies and small excitation amplitudes. The drop in the current in (a) corresponds to the negative conductance in (b).

After checks of the spectral behavior of the transmission coefficients, current densities and AC properties, one can proceed to integrate these spectral properties over energy and obtain observable quantities, such as current and conductance. In Figure 4, the first results of an AC small signal conductance versus voltage characteristic in combination with the static DC current voltage characteristic are presented. As expected, the low frequency conductance does show a large negative peak in the region where the DC current drops as a function of voltage. A similar curve could be obtained by taking a numerical differential of the DC current voltage characteristic. The low frequency AC conductance gives therefore, results that were anticipated from a quasi-static DC analysis using a very different method! At this time, we have not introduced all the correct scaling constants into the AC conductance and leave the plot on arbitrary units. Also, we were not able to fully analyze the imaginary part of the AC admittance and defer this to the next reporting period.

Finally, we checked the frequency behavior of the conductance. Physically, one would expect the RTD to dramatically change its characteristics when the AC field changes at a time-scale that corresponds to the lifetime of the resonance. This lifetime is dependent on the actual design of the RTD and depends exponential on the barrier thickness. In the case of our test structure NEMO predicts a resonance width of about 2meV which corresponds to a lifetime of the state of about 330fs. That means we can expect a change in the intrinsic conductance behavior at a frequency of about 3THz for our test structure.

Figures 5a and 5b depict the conductance through the test RTD as a function of bias and frequency in a 3D surface plot from two different vantage points. Evident at low frequencies are two conductance extrema, a soft maximum at 0.3V and a sharp minimum at 0.34V. These two conductance extrema are frequency independent for a wide frequency range. However, above a certain cutoff frequency both conductance extrema vanish. Shown in Figure 5c is a 2D slice through the 3D surface at a constant voltage of 0.34V, which corresponds to the conductance minimum at low frequencies. The negative conductance is shown to cut off at 3-4 THz as expected by the RTD's resonance width and corresponding lifetime.

*For the implementation of the AC small signal simulation we conclude from our first results that the simulations "make sense" in that they provide physical answers.*

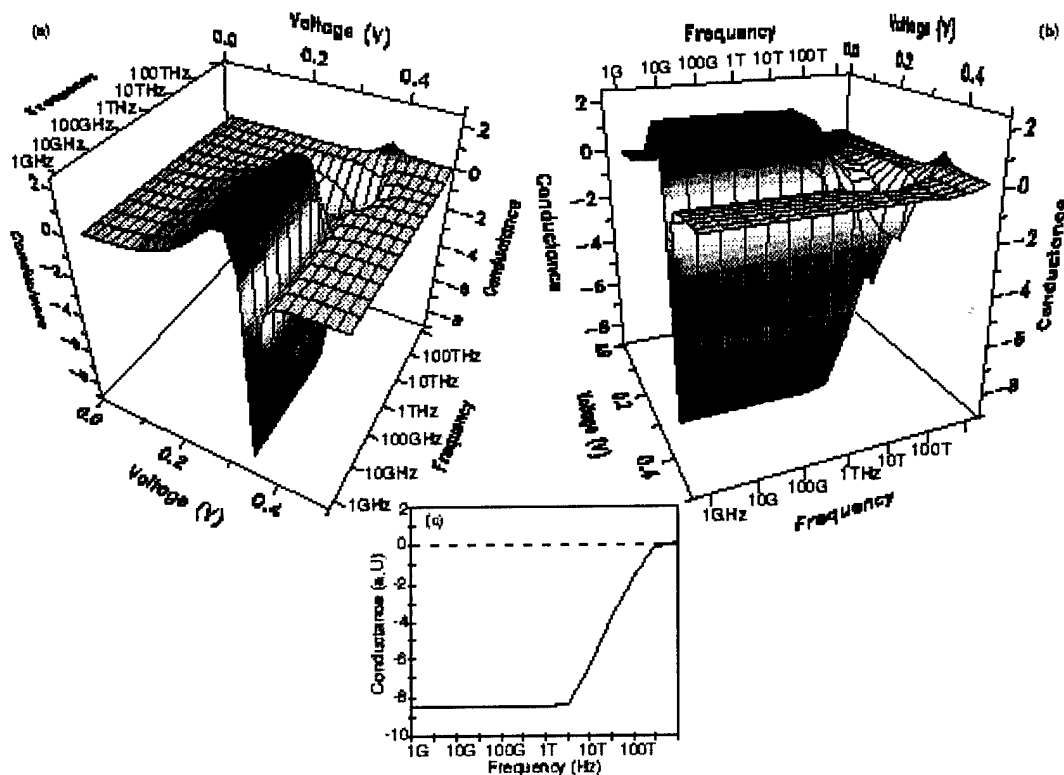


Figure 5. (a, b) Conductance as a function of applied voltage and frequency viewed from different vantage points. The negative conductance vanishes as the frequency is increased. (c) Cut through (a, b) at a voltage of 0.34V at the minimum of the negative conductance. The natural resonance width of the RTD in this example is about 2meV, which corresponds to a lifetime of 300fs, or a cutoff frequency of 3THz.

### **Task 3. Design Architecture of 2D/3D, Steady-State/Transient, Quantum/Hydrodynamic CAD Tool**

A new architecture for the quantum simulator is being planned so the tool can incorporate more physics while at the same time become more portable, more flexible for future development, and easier to support as a commercial tool. Along these ends a CFDRC employee spent three weeks at JPL to learn more of the theory and source code construction of NEMO. The source code was reorganized into a directory structure, and was put under version control to allow sharing of the source code amongst the different institutions involved (CFDRC, JPL, Raytheon). Also, to increase the code's portability a new build system was implemented and the code was ported to the DEC platform.

#### **Version Control**

The quantum simulator is based on the NEMO simulator. The NEMO tool is a large software package that requires further support from the original authors. To establish a fruitful cooperation between CFDRC and JPL a "universal" source has been established that all parties will develop from. The "universal" source to be developed and marketed during the SBIR project has been put under version control using CVS software. This version control software can handle

complex directory structures, multiple file types, tracks file and directory changes, deal with multiple users, and can be accessed over a remote network. The established CVS repository will enable CFDRC, JPL, and Raytheon to develop from the same source files. Thus all parties benefit from others development.

The approximately 960 NEMO source code files that have been kept in a single working directory are now grouped into a library oriented directory tree. During the past 5 years of NEMO software development efforts were made to create modular, structured code that can easily be expanded. As the code was growing in size to approximately 250,000 lines module inter-dependencies began to develop. These module inter-dependencies prevented compilation of the code into distinct libraries and prevented new developers to the code to see the structure in the massive amount of files. Careful debugging and de-tangling separated the source code into distinct groups. The code has now been ordered into the following packages: 1) system utilities, 2) i/o, 3) math, 4) material, 5) database, 6) material-database, 7) drivers, and 8) graphical user interface. These are hierarchical libraries and not stand alone libraries. The libraries depend on function calls from libraries at the beginning of the hierarchy so a library labeled with a particular number depends on libraries labeled with lower numbers. The libraries are now stored in different directories and are available as building blocks for future work.

### **Portability**

A new build system was implemented for the source code that replaces the 320+ files that were previously used to build the source on different platforms. The new build system uses a perl script to establish the file dependencies and build rules of the source files to be compiled and linked. The perl script allows the same build method on windows based as well as UNIX based platforms. A shell script is then used to determine the platform specific compile and link flags necessary for a successful build of the desired form of the NEMO software application and libraries. The shell 'mk' script collects the proper compiler and links calls for the different platforms where NEMO will be built into one file.

The NEMO source has been ported to a DEC platform making the software available on one more platform. Some of the changes required for the port included

- A mass initialization error that caused problems only on the DEC build was fixed.
- NEMO had defined a complex square root routine similar in name to one defined in the lapack libraries. Lapack libraries were linking with NEMO's routine instead of lapack routines causing errors. The NEMO function was renamed so the lapack routines would link with the lapack routine and not the NEMO one.
- Other errors arising in the Lapack routines used to solve the linear equations were corrected by compiling the libraries at a lower optimization and using the newer release version of the lapack code.

### **Theory and Source Training**

A CFDRC employee (Phillip Stout) spent three weeks at JPL to gain an understanding of NEMO theory and source code construction from some of the original authors of the code (Gerhard

Klimeck and R. Chris Bowen). NEMO provides the user with a wide variety of bandstructure, charging and scattering models. The charging models are shared amongst all bandstructure and scattering models as they establish the potential landscape. Scattering and non-scattering models build the two underlying simulation groups. All non-scattering models use the same integration, resonance finding, grid generation and recursive Green function algorithms. JPL provided an introduction to all these core routines in the non-scattering software block. Of particular importance, the main routines in NEMO that will be effected by the small signal AC implementation were reviewed. Connections were made between variables in the mathematical discussion of NEMO with the variable names and C structures used in the code. Also, some time was spent writing a moving average routine which averages NEMO generated data onto a uniform plotting grid. Writing the needed routine helped the trainee in understanding NEMO I/O and internal data structures.

### **3. DIFFICULTIES/PROBLEMS**

No difficulties or problems were encountered during this reporting period.

### **4. PLANS FOR NEXT REPORTING PERIOD**

- Finish single band AC model such that all the correct integration constants are used. The conductance will be correct in its absolute values as well.
- Debug the 2 and 10 band AC simulations, provide correct integration constants and achieve correct absolute conductance values.
- Evaluate the imaginary part of the admittance to extract capacitive and inductive properties of the RTD.
- Verify the multiband AC boundary conditions implemented at JPL with theory to be derived at Raytheon.
- Presently the AC observables are obtained in the Tsu-Esaki approximation in a single energy integration. To reach quantitative agreement with experiment as shown in Figure 1a and 1b, a numerical integration over transverse momentum must be introduced. This numerical integration is presently not performed for the AC observables, but will be implemented next.

### **5. SCHEDULE**

The project schedule is shown in Table 1.

Table 1. Work Schedule

TASK DESCRIPTION	Months After Receipt of Contract								
	1	2	3	4	5	6	7	8	9
Task 1. Implement AC Small Signal Analysis	■	■	■	■					
Task 2. Demonstration/Validation					■	■			
Task 3. Design Architecture	■	■	■	■	■	■			
Task 4. Final Report						■	■		
Task 5. Solve Drift Diffusion (OPTION)							■	■	■
Task 6. Experimental Validation (OPTION)							■	■	■

Work Completed
  Work to be Done

## 6. REFERENCES

- Fernando, C. L. and Frensley, W. R. (1995), "Intrinsic high-frequency characteristics of tunneling heterostructure devices," *Phys. Rev. B*, 52 (7), pp. 5092-5104.
- Klimeck, G., Lake, R., Bowen, R. C., and Frensley, W. R. (1995b), "Quantum device simulation with a generalized tunneling formula," *Appl. Phys. Lett.*, 67 (17), pp. 2539-2541.
- Lake, R., Klimeck, G., Bowen, R. C., and Jovanovic, D. (1997), "Single and multiband modeling of quantum electron transport through layered semiconductor devices," *J. App. Phys.* 81 (2), pp. 7845-7869.